GVF-Based Anisotropic Diffusion Models

Hongchuan Yu, *Member, IEEE,* and Chin-Seng Chua, *Member, IEEE*

Abstract—In this paper, the gradient vector flow fields are introduced in image restoration. Within the context of flow fields, the shock filter, mean curvature flow, and Perona-Malik equation are reformulated. Many advantages over the original models can be obtained; these include numerical stability, large capture range, and high-order derivative estimation. In addition, a fairing process is introduced in the anisotropic diffusion, which contains a fourth-order derivative and is reformulated as the intrinsic Laplacian of curvature under the level set framework. By applying this fairing process, the shape boundaries will become more apparent. In order to overcome numerical errors, the intrinsic Laplacian of curvature is computed from the gradient vector flow fields instead of the observed images.

Index Terms—Anisotropic diffusion models, gradient vector flow (GVF) fields, intrinsic laplacian of curvature.

I. INTRODUCTION

THE image anisotropic diffusion is to smooth the image in the direction of an edge, but to not be perpendicular to it, so that the location and strength of the edges can be maintained. Since the Perona–Malik equation was presented as an anisotropic diffusion model in [1], there has been extensive literature that presents various anisotropic diffusion models and offers diverse numerical schemes to obtain the steady-state solutions [2]–[10]. In this paper, we will emphasize the following three classical image restoration models: shock filter, mean curvature flow scheme, and the Perona–Malik equation.

The shock filter scheme was presented in [12] as a stable deblurring algorithm which approximates a deconvolution. Unfortunately, this scheme is extremely sensitive to noise. Further research has therefore focused on defining a more precise and robust coefficient function in an attempt to smooth noise while preserving the shape and geometric features. The common approach is to add some kind of an anisotropic diffusion term, as a weighting factor, between the shock and the diffusion processes. A combination to couple shock with a diffusion term was proposed [2], $I_t = -\text{sign}(G_\sigma * I_{\eta\eta})|\nabla I| + cI_{\xi\xi}$, where c is a positive scale, η is the direction of gradient, and ξ is the direction perpendicular to the gradient. In [4], a complex diffusion model was presented $I_t = -(2/\pi)\arctan(a\,\text{Im}(I/\theta))|\nabla I| + \alpha_1 I_{\eta\eta} +$

$\alpha_2 I_{\xi\xi}$, where the first term is a shock term, a is a parameter that controls the sharpness, and $\alpha_1 = re^{i\theta}$ and α_2 are, respectively, complex and real scaling factors.

The mean curvature flow model was presented in [8] and [16] as an edge enhancement algorithm in the presence of noise. In [10], the mean curvature flow was applied to enhance and denoise under the Min/Max flow scheme. In their applications, only the pure curvature flow model was employed. In [7], a deconvolution model was further introduced in the mean curvature flow model for deblurring and denoising.

A further enhancement to the Perona–Malik equation is the ability to weight the terms $I_{\eta\eta}$ and $I_{\xi\xi}$ adaptively. In [5], the coefficient function was defined as $g(x) = (1 + x/k_1)^n)^{-1} - \alpha\left(1 + ((x - k_2)/w)^{2m}\right)^{-1}$, where k_1 is a threshold for gradients to be smoothed out, k_2 and w are, respectively, threshold and range factors that control the inverse diffusion process. In [6], the general form of the Perona–Malik equation was presented $I_t = c(aI_{\eta\eta} + bI_{\xi\xi})$. The eigenvalues of the Hessian matrix are regarded as the second-order directional derivatives $I_{\eta\eta}$ and $I_{\xi\xi}$. The two corresponding eigenvectors are considered to be the directions of $I_{\eta\eta}$ and $I_{\xi\xi}$, respectively, so as to suppress the influence of noise. From the above discussion, it can be seen that the research focus is to design a coefficient function that should be robust, simple, and controlled.

In this paper, the gradient vector flow (GVF) fields [11] are incorporated with the anisotropic diffusion. Since these flow fields can be determined in advance (that is, they are invariable during image diffusion), and can also provide a large capture range to the object boundaries, they perform well on noise or spurious edges. Another particular advantage is the improvement of the high-order derivative estimation. We will demonstrate these advantages by applying the GVF fields to the shock filter, the mean curvature flow, and the Perona–Malik equation. These models are chosen for comparison because many of the earlier image restoration models usually regard these three models as their basic prototypes. In addition, with the aim of making the enhanced boundaries vivid, the fourth-order flow model of the plane curve [13] is introduced in the anisotropic diffusion. The GVF fields make the fourth-order flow computation simple and reliable. Our research in this paper is also inspired by the work in [24], in which the anisotropic diffusion model is applied to smooth and denoise the normal vector fields of a three-dimensional (3-D) surface. In this paper, we extend their work to implement image enhancement and denoising based on normal vector fields, that is, the GVF fields.

This paper is organized as follows: Section II briefly introduces the GVF fields. In Section III, the shock filter, mean curvature flow, Perona–Malik model, and the fourth-order flow model are reformulated in terms of the GVF fields. The implementation of our proposed models and experimental results is shown

H. Yu was with the School of Electrical and Electronics Engineering, Nanyang Technological University, Singapore 639798. He is now with the School of Computer Science and Software Engineering, University of Western Australia, Perth, WA 6009, Australia (e-mail: cnyuhc@yahoo.com).

C. S. Chua is with the School of Electrical and Electronics Engineering, Nanyang Technological University, Singapore 639798 (e-mail: ecschua@ntu.edu.sg).

in Section IV. Finally, Section V concludes with some ideas for future research.

II. GVF FIELDS

The GVF field was first presented for active contour models, in which the GVF field was used as an external force [11]. The GVF fields are computed as a diffusion of the intensity gradient vectors that enable noise to be suppressed. Since the GVF is estimated directly from the continuous gradient vector space, its measurement is contextual and not equivalent to the distance from the closest point. In addition, the GVF provides a bidirectional forcefield that can capture the object boundaries from either side without any prior knowledge of shrinking or expanding toward the object boundaries. Hence, the GVF fields can provide a large capture range to the object boundaries.

First, a Gaussian edge detector (zero mean, with σ_E variance) is used in the edge map [14], $f(\mathbf{x}) = 1 - (1/\sqrt{2\pi}\sigma_E)\exp\left(-|\nabla(G_\sigma * I)(\mathbf{x})|^2/2\sigma_E^2\right)$, $\mathbf{x} \in R^2$, where G_σ is a Gaussian with a small variance. Compared with other forms of the edge map in [11], this form could avoid the case where the norm of the GVF vector decreases quickly during the evolution of the GVF fields. Indeed, this is only a normalization process. Since the magnitude of the GVF is spatially varying and is usually not unity, the GVF is normalized in order to make the maximum magnitude unity. The GVF field $\vec{\mathbf{v}}(\mathbf{x})$ is defined as the equilibrium solution to the following vector diffusion equation:

$$\begin{cases} \vec{\mathbf{v}}(\mathbf{x},t)_t = \mu\nabla^2\vec{\mathbf{v}}(\mathbf{x},t) - (\vec{\mathbf{v}}(\mathbf{x},t) - \nabla f(\mathbf{x}))|\nabla f(\mathbf{x})|^2 & (1a) \\ \vec{\mathbf{v}}(\mathbf{x},0) = \nabla f(\mathbf{x}) & (1b) \end{cases}$$

where μ is a blending parameter. In (1a), the first term on the right is the smoothing term since it will produce a smoothly varying vector field. Since μ is constant, smoothing occurs everywhere. The second term on the right of (1a) is the data term since it encourages the vector field $\vec{\mathbf{v}}(\mathbf{x})$ to be close to $\nabla f(\mathbf{x})$. It should be noted that $|\nabla f(\mathbf{x})|^2$ grows large near strong edges and should dominate at the boundaries. In [22], other choices for parameters μ and $|\nabla f(\mathbf{x})|^2$ are proposed. In reality, the smoothing term extends the gradient map further away from the edges so as to enlarge the capture range, and simultaneously suppresses the influence of noise (see [22] for details). In Fig. 1, the vectors $\vec{\mathbf{v}}(\mathbf{x})$ in the GVF fields always point to the closest boundaries of the object. Note that the vector $\vec{\mathbf{v}}(\mathbf{x})$ does not always maintain the same direction with the intensity gradient but will always point to the closest boundary. On both sides of the boundary, the directions of the GVF vectors will be opposite. Moreover, a large capture range to the desired edges is achieved through a diffusion process of the intensity gradient vectors, which do not smooth the edges themselves. In the anisotropic diffusion models, the second- or higher-order derivative is usually needed. In general, the high-order derivative is very sensitive to noise or computational error. Hence, the intuitional motivation of introducing the GVF fields is to decrease the order of the derivative.
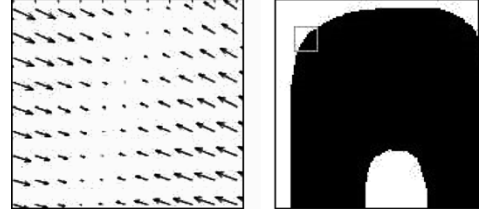
Fig. 1.   GVF field corresponding to the rectangle on the right image.

Since the GVF fields are invariable during the image diffusion, they can be determined in advance. This will decrease the influence of noise and improve the numerical stability for image evolution.

In order to reveal the intrinsic properties of the GVF fields, $\nabla f(|\nabla I|)$ can be rewritten as

$$\vec{\mathbf{v}}(\mathbf{x}) = \nabla f(|\nabla I(\mathbf{x})|) = \lambda_1 \nabla|\nabla I(\mathbf{x})| \qquad (2)$$

where $\lambda_1 = \left(|\nabla I|/\sqrt{2\pi}\sigma_E^3\right)\exp\left(-|\nabla I|^2/2\sigma_E^2\right) > 0$. For convenience, the Gaussian operator G_σ in $f(\mathbf{x})$ is omitted. Strictly speaking, the vector field $\vec{\mathbf{v}}(\mathbf{x})$ is only an approximation of $\nabla f(\mathbf{x})$, which is computed from the observed image data, with the exception that noise or trivial details can be suppressed. Although the GVF fields will be applied to several nonlinear models (with different geometrical interpretations) in Sections III and IV, it is essentially an approximation and not an equivalence. For simplicity, we still use the equal sign in (2).

III. DIFFUSION MODELS BASED ON GVF FIELDS

A. Shock Filter

The heat equation will result in a smoothing process, while the inverse heat equation will lead to a deblurring process to approximate deconvolution. However, the inverse heat equation is extremely ill-posed. The shock filter tries to get as close as possible to the inverse heat equation to reach a stable solution. This is formulated as $I_t = -\mathrm{sign}(I_{\eta\eta})|\nabla I|$, where η is the direction of the gradient.

In this section, the GVF fields are introduced in the shock filter. Both sides of (2) are dot-multiplied by the intensity normal vector $\mathbf{N} = \nabla I/|\nabla I|$ as

$$\vec{\mathbf{v}} \cdot \mathbf{N} = \lambda_1 \nabla|\nabla I| \cdot \mathbf{N} = \lambda_1 \left\langle D^2 I \frac{\nabla I}{|\nabla I|}, \mathbf{N} \right\rangle \qquad (3)$$

where $D^2 I$ denotes the Hessian of intensity I. It can be noted that the above equation can effectively approximate the second derivative of I in the direction of the intensity gradient $I_{\eta\eta}$ up to a positive scale factor λ_1. So the shock filter equation can be reformulated as

$$I_t = -\mathrm{sign}(\vec{\mathbf{v}} \cdot \mathbf{N})|\nabla I|. \qquad (4)$$

According to the GVF definition in Section II, the direction of the GVF vector will change across the boundaries while one of the gradients will be unchanged. Therefore, the sign of $(\vec{\mathbf{v}} \cdot \mathbf{N})$ will be opposite for both sides of the boundaries. This will result in two opposite evolutions for both sides of boundaries. Thus, (4) allows the image to develop true edges. The worst case is

when the GVF is tangential to the intensity normal and no further evolution takes place. From the implementation point of view, (4) simplifies the computation of $I_{\eta\eta}$. As a matter of fact, the original shock filter scheme is extremely sensitive to noise because of the lack of the diffusion processes (see [4] for details). While the term $(\vec{v} \cdot \mathbf{N})$ in (4) is only a second derivative of I in the direction of the intensity gradient and not a diffusion term, it cannot be used to remove noise. Thus, the noise-sensitive problem will still exist in (4) as in the original scheme.

B. Mean Curvature-Flow Equation

The mean curvature-flow equation is only one of the anisotropic diffusion models. The key idea is that an image is interpreted as a collection of isointensity contours, which can be evolved. Usually its standard form can be formulated as $I_t = \kappa|\nabla I|$, where κ is the curvature of isointensity contours $\kappa = \nabla \cdot (\nabla I/|\nabla I|)$. It has received a lot of attention because of its geometrical interpretation. The level sets of the solution move in the normal direction with a speed proportional to their mean curvature. Many theoretical aspects of this evolution equation, such as the theory of weak solutions based on the viscosity solution theory, have been summarized in [15]. In nonlinear image diffusion applications, it has been proven that the curvature flow equation is well posed and the curvature flow has been used as an image selective smoothing filter in [8] and [16]. However, according to Grayson's theorem [15], all structures would eventually be removed through continued application of the curvature-flow scheme. In order to preserve the essential structures while removing noise, the Min/Max flow framework based on the curvature flow equation was proposed in [10]. In the above algorithms, only the pure mean curvature flow model is used. Indeed, we could introduce some constraint terms in the mean curvature-flow scheme just as in the active contour models. In this section, our starting point is to balance between the internal force, which is from the curvature of evolution curve, and the external force. The GVF fields will provide the curvature-flow scheme with a new external force, which can overcome the noise or spurious edges effectively.

Consider (3): $(\vec{v} \cdot \mathbf{N})$ indicates that the second derivative of I is in the direction of gradient. The sign of $(\vec{v} \cdot \mathbf{N})$ will change along the normal to the boundaries in the neighborhood even if the direction of gradient $\mathbf{N}$ does not change. Thus, the GVF indicates a correct evolution direction of the curvature flow rather than the gradient direction. In our approach, the GVF is introduced as a new external force into the original curvature evolution equation, directly from a force-balanced condition. According to (3), we determine a contextual flow $C_t = (\vec{v} \cdot \mathbf{N})\mathbf{N}$, where $C \in R^2$. An important fact is that the propagation driven by the curvature flow always takes place in the inward normal direction (that is, $-\mathbf{N}$). It is clear that a better way to reach the boundaries is to move along the direction of GVF. Due to noise or spurious edges, the gradient vector cannot always align to the GVF. Thus, a desired propagation can be obtained when the vector of $\vec{v}(\mathbf{x})$ and the inward normal direction are identical. On the other hand, the worst case occurs when $\vec{v}(\mathbf{x})$ is perpendicular to the normal (that is, $\vec{v} \perp \mathbf{N}$). Since $\vec{v} \cdot \mathbf{N} = 0$ in this case, the GVF will lose its effect.

Under the level set framework, it is convenient to introduce this contextual flow from the GVF fields into the curvature evolution equation

$$I_t = r\kappa|\nabla I| - (1 - r)\vec{v} \cdot \nabla I \qquad (5)$$

where $0 \leq r \leq 1$. When the GVF and the inward normal have the same directions, then the flow will be accelerated. On the other hand, when these vectors have opposite directions, the flow will be weakened, or even stopped. When the GVF is tangential to the normal, then the curvature flow κ will dominate the evolution process.

The proposed scheme of (5) is similar to the model presented in [7], in which a model of convolution was introduced in the mean curvature-flow scheme. Indeed, both the deconvolution and deblurring processes are sensitive to noise, while the mean curvature term could make them well posed (see [7] for details).

From an implementation perspective, the scheme of (5) has an advantage over the original curvature evolution equation: due to the invariance of the GVF fields, the flow would not propagate endlessly. When a balance between the internal and external force is reached, the flow evolution will be terminated at the object boundaries. Furthermore, since the GVF fields provide a large capture range to the object boundaries, the flow would not fall at the noise points or spurious edges. Thus, the scheme of (5) is able to suppress noise effectively.

C. Perona–Malik Equation

The Perona–Malik equation (P–M equation), introduced in [1], has been successful in dealing with image restoration in a wide range of images. The key idea is to roughly smooth out the irrelevant, homogeneous regions (such as the heat equation) when $|\nabla I|$ is small and to enhance the boundaries instead (such as an inverse heat equation) when $|\nabla I|$ is large. The P–M equation, in the divergence form, is $I_t = \nabla \cdot (g(|\nabla I|)\nabla I)$ and $I(t = 0) = I_0$. In this equation, $g(\cdot) > 0$ is a smooth decreasing function of the gradient $|\nabla I|$, which is usually defined as an exponential expression $g(|\nabla I|) = \exp(-|\nabla I|^2/2\sigma^2)$, where σ is a positive parameter that controls the level of contrast at the boundaries. The coefficient function $g(|\nabla I|)$ is close to one for $|\nabla I| \ll \sigma$, while $g(|\nabla I|)$ is close to zero for $|\nabla I| \gg \sigma$. A theoretical analysis shows that solutions of the P–M equation can perform an inverse diffusion near boundaries and enhance edges that have gradients greater than σ. However, the design of the coefficient function to balance between the smoothing and inverse diffusion processes is critical. Nevertheless, the original P–M equation is an ill-posed parabolic equation. In [23], the coefficient function $g(|\nabla I|)$ was replaced by $g(|G_\sigma * \nabla I|)$ which leads to a well-posed model, and this has been widely used in practice. In this section, the GVF fields are also introduced in the well-posed P–M model. For convenience, we will omit the Gaussian operator G_σ in $g(|G_\sigma * \nabla I|)$. As the GVF is determined in advance, the influence of noise or spurious edges will be weakened in the inverse diffusion process. In this section, we will try to design the coefficient functions of the smoothing term and inverse diffusion term based on the GVF fields, respectively, so that the two functions could be adjusted independently and freely for different smoothing effects.

First, let us expand the P–M equation

$$I_t = g'|\nabla I|I_{\eta\eta} + g\Delta I$$

where η is the direction of gradient. In general, the first term is an inverse diffusion term for sharpening the boundaries while the second term is a Laplacian term for smoothing the regions that are relatively flat. In accordance with the GVF definition, the coefficient function is defined as $g(|\nabla I|) = 1 - f(|\nabla I|) = (1/\sqrt{2\pi}\sigma_E)\exp\left(-|\nabla I|^2/2\sigma_E^2\right)$. Comparing (2) with the P–M equation, we note that the gradient vector ∇I is missing in (2). Indeed, the P–M equation is hybrid and combines the gradient vector ∇I and the estimate of gradient $|G_\sigma * \nabla I|$. Consider the equation $-\vec{v} \cdot \nabla I = g'|\nabla I|I_{\eta\eta}$. The term $(-\vec{v} \cdot \nabla I)$ is an approximation of the inverse diffusion term in the P–M equation. Thus, the P–M equation can be rewritten as

$$I_t = -\vec{v} \cdot \nabla I + g\Delta I \qquad (6)$$

where $g(\cdot)$ can be controlled independently. The advantages of (6) over the traditional P–M equation are distinct.

- Since only the gradient needs to be computed directly from the observed images in the inverse diffusion term, this will improve the robustness of the inverse diffusion term.
- The worst case for the first term is when the GVF is tangential to the gradient direction, then this inverse diffusion term is equal to 0. In fact, it is noise or spurious edges that cause these vectors to be orthogonal. Thus, the regions around these points should be smoothed and should not be enhanced.
- The scheme of (6) is an open framework. Under this scheme, the inverse diffusion term and Laplacian term can be easily controlled by redefining their coefficients $g(\cdot)$ and $g'(\cdot)$, according to the smoothing effect.

Consider the coefficient function $g(x)$ and its derivate $g'(x)$. By adjusting the parameter σ_E, the smoothing effect is controlled. But the coefficient of the inverse diffusion term cannot be adjusted freely (Fig. 2) since the GVF fields have been determined before image evolution. An intuitional idea is to deform $g'(x)$ to become similar to the Gaussian function. A robust method is to redefine the coefficient of the inverse diffusion term as $\hat{g}(x) = sx^m g'(x), m \geq 1$, where s is a scaling factor and m is a parameter that controls the location of the wavecrest. This function is a bimodal function, in which each wavecrest is similar to the Gaussian distribution. Since $x = |\nabla I|$ in our case, we only need to consider a single wavecrest of this function. From the definition of $\hat{g}(x)$

$$\hat{g}(x) = sx^m g'(x) \cdot \exp\left(-\frac{(a^2 - 2ax)}{2\sigma_E^2}\right)$$
$$\cdot \exp\left(-\frac{(2ax - a^2)}{2\sigma_E^2}\right)$$
$$= -\frac{sx^{m+1}}{\sqrt{2\pi}\sigma_E^3}\exp\left(-\frac{(x-a)^2}{2\sigma_E^2}\right)$$
$$\cdot \exp\left(-\frac{(2ax - a^2)}{2\sigma_E^2}\right).$$

Since x^m in $\hat{g}(x)$ is a power function, it can eliminate the influence from the exponential term $\exp\left(-(2ax - a^2)/2\sigma_E^2\right)$ for the noise points with large gradient magnitudes. It can be noted
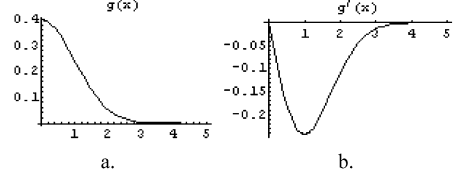
Fig. 2. Comparison of the coefficients $g(x)$ and $g'(x)$, plotted as the functions of gradient magnitude. ($\sigma_E = 1$).
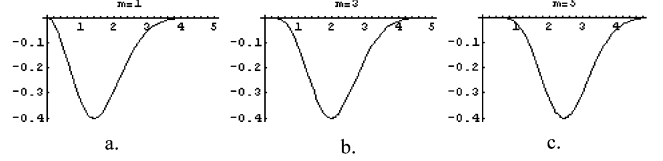
Fig. 3. Coefficient $\hat{g}(x)$ varies with parameter m **AUTHOR: INSERT "WHICH"?** changed ($\sigma_E = 1$).

Fig. 4. Evolution of star shape. (a) Flow under the intrinsic Laplacian of curvature with iteration $= 15\,000$. (This example is from [21]). (b) Flow under the mean curvature with iteration $= 1000$.

that $x = a$ is a new center for the coefficient function of the inverse diffusion term. When parameter m is increasing, the center of the coefficient function $\hat{g}(x)$ will be moved from low to high. This is illustrated in Fig. 3.

Thus, the extension of (6) can be re-expressed as

$$I_t = -s|\nabla I|^m \vec{v} \cdot \nabla I + g\Delta I, \quad m \geq 1 \qquad (7)$$

where the parameter m controls the inverse diffusion, the parameter σ_E controls the smoothing effect, and these two parameters are independent of each other.

The scheme of (7) is only one of the various forms of the P–M equation. The scheme of (6) is an open framework, in which there are many possible choices for designing the coefficient functions $g(x)$ and $g'(x)$.

D. Fairing Processing and Fourth-Order Flow Model

The fairing process is derived from computer-aided-design (CAD)/computer-aided-modeling (CAM) modeling techniques. A basic approach is to minimize the two energy functions; that is, $\min \int_L \kappa^2 ds$ for curve fairness and $\min \int_S \left(\kappa_1^2 + \kappa_2^2\right) ds$, where κ_1 and κ_2 are the principle curvatures for surface fairness [17]. They are usually called the least total curvature. Recently, these curvatures were introduced [19], [20] in the anisotropic diffusion model for the curve and surface. The main idea is to smooth complicated noisy surfaces, while preserving sharp geometric features. Under a variational framework, fourth-order PDEs can be deduced from the least total curvature. In this section, we focus on the fourth-order flow model in the plane, which will be introduced in the image anisotropic diffusion.

In [21], the fourth-order flow was presented as the intrinsic Laplacian of curvature under the level set framework

$$\kappa_{ss} = \frac{\left(\kappa_{xx}\phi_y^2 - 2\kappa_{xy}\phi_x\phi_y + \kappa_{yy}\phi_x^2\right)}{\mathrm{grad}^2} - \kappa\frac{\left(\kappa_x\phi_x + \kappa_y\phi_y\right)}{\mathrm{grad}}$$

where $\mathrm{grad} = \sqrt{\phi_x^2 + \phi_y^2}$. This is the second derivative of the local curvature κ with respect to the arc length parameter s. The particular geometric property of this flow is to improve the isoperimetric ratio, but not to reduce the enclosed area such as the mean curvature flow. For comparison, the evolutions of a star shape under the intrinsic Laplacian of curvature flow $I_t = \kappa_{ss}|\nabla I|$ and the mean curvature flow $I_t = \kappa|\nabla I|$ are shown in Fig. 4.

It is obvious that the flow under the intrinsic Laplacian of curvature will finally converge to a circle. This is due to the isoperimetric ratio of the circle being maximum when the perimeter is fixed, and that the derivatives of the curvature converge uniformly to zero. Thus, the final solution to the flow under the intrinsic Laplacian of curvature should be a circle. In image diffusion, this fourth-order flow model will preserve the boundaries of shapes and not smooth them out. Simultaneously, some small oscillations around the boundaries will be smoothed out.

However, owing to the fourth-order derivative term in the intrinsic Laplacian of curvature, it becomes highly sensitive to errors and the fourth-order derivative term requires the numerical scheme with very small time steps. In Fig. 4(a), the space step $\Delta x = 0.0667$ and the time step $\Delta t = 5 \times 10^{-6}$ with more than 40 reinitializations are used. In fact, it is ill-posed to minimize the total squared curvature $\int_L \kappa^2 ds$ in the plane-closed curves (that is, plane curve raveling). Since the total squared curvature is scale dependent, it can be reduced as far as the gradient flow inflates any closed curve without limit. In order to make it well posed, the total squared curvature was modified to $\int_L (\kappa^2 + \alpha^2)ds$ [13] and the corresponding gradient flow was deduced under a variational framework

$$C_t = \left(\kappa_{ss} + \frac{\kappa(\kappa^2 - \alpha^2)}{2} \right) \mathbf{N} \qquad (8)$$

where C is a closed curve, $\mathbf{N}$ is the normal vector, and $\alpha \neq 0$ is the penalty function to make the problem well posed. Few important conclusions to **AUTHOR: "FROM" INSTEAD OF "TO"?**(8) from **AUTHOR: "TO" INSTEAD OF "FROM"?** [13] need to be highlighted as follows.

- The long time solution of (8) exists and a stationary solution can be reached.
- If the descent flow corresponding to the "pure" energy $\int_L \kappa^2 ds$ is considered, the normal speed is simply $F = \kappa_{ss} + \kappa^3/2$.
- The flow can smooth the embedded curves as well as the immersed curves.

The intrinsic Laplacian of curvature was introduced in active contours as a frigid force for 2-D and 3-D segmentation in [18]. In fact, it could also be applied in the anisotropic diffusion of images. Due to the isoperimetric property originating from the intrinsic Laplacian of curvature term, the shape boundaries in the evolving image will become vivid. We will deduce the intrinsic Laplacian of curvature directly from the GVF fields to improve numerical stability.

Consider the GVF form of (3). The second derivative of I is extracted in the direction orthogonal to the gradient. The derivative can be formulated as $\lambda_1 I_{\xi\xi} = \lambda_1 \Delta I - \vec{v} \cdot \mathbf{N}$.

As $I_{\xi\xi}$ can be written as a "quasi divergence form" in [16], $I_{\xi\xi} = |\nabla I|\nabla \cdot (\nabla I/|\nabla I|)$, we have, $\lambda_1 \Delta I - \vec{v} \cdot \mathbf{N} \equiv \lambda_2 \hat{\kappa}$,

where $\lambda_2 = |\nabla I|\lambda_1 > 0$, $\hat{\kappa} = \nabla \cdot (\nabla I/|\nabla I|)$, which can be looked upon as a curvature flow. In general, the curvature flow evolves along the direction of a gradient. The above equation can be defined as a force field along the direction of gradient $\mathbf{E} = \lambda_2 \hat{\kappa} \mathbf{N}$. The derivative of the field $\mathbf{E}$ with respect to the arc length follows from the Frenet–Serret formulation

$$\mathbf{E}_s = (\lambda_2 \hat{\kappa})_s \mathbf{N} - (\lambda_2 \hat{\kappa}) \kappa \mathbf{T}$$

where $\mathbf{T}$ is a unit tangent vector and $\mathbf{T} \cdot \mathbf{N} = 0$, κ is the isointensity contour curvature, which is extracted only from the observed images. The second derivative of the field $\mathbf{E}$ with respect to the arc length is

$$\mathbf{E}_{ss} = \left((\lambda_2 \hat{\kappa})_{ss} - (\lambda_2 \hat{\kappa})\kappa^2\right) \mathbf{N} - (2(\lambda_2 \hat{\kappa})_s \kappa + (\lambda_2 \hat{\kappa})\kappa_s)\mathbf{T}.$$

For the gradient flow, we have $\mathbf{E}_{ss} \cdot \mathbf{N} = (\lambda_2 \hat{\kappa})_{ss} - (\lambda_2 \hat{\kappa})\kappa^2$. Note that this is the normal speed of the gradient flow corresponding to the "pure" energy $\int_L \kappa^2 ds$. Denoting $K = \lambda_2 \hat{\kappa}$ for convenience, the second derivative of K can be expressed as

$$K_{ss} = \frac{(K_{xx}I_y^2 + K_{yy}I_x^2 - 2K_{xy}I_xI_y)}{\mathrm{grad}^2} - \kappa \frac{(K_xI_x + K_yI_y)}{\mathrm{grad}}$$

where $\mathrm{grad} = \sqrt{I_x^2 + I_y^2}$, K can be estimated from the GVF and the observed image, and λ_2 can be estimated by using the gradient $|\Delta I|$ from the observed image data and λ_1 from the GVF fields. Hence, the flow under the intrinsic Laplacian of curvature is rewritten as

$$I_t = -(\mathbf{E}_{ss} \cdot \mathbf{N})|\nabla I| = \left(K\kappa^2 - K_{ss}\right)|\nabla I|.$$

The fourth-order derivative term K_{ss} and the related term K in the above intrinsic Laplacian of curvature flow are estimated from the GVF fields and are not extracted directly from the observed image. This effectively improves the numerical stability.

However, the above intrinsic Laplacian of curvature flow equation is ill posed. Compared with the scheme of (8), it lacks a mean curvature term. In order to make it well posed, the mean curvature flow is coupled with the above equation as

$$I_t = \beta\kappa|\nabla I| + \left(K\kappa^2 - K_{ss}\right)|\nabla I| \qquad (9)$$

where β is a constant that balances the contribution between the mean curvature flow and the fourth-order flow.

IV. Experiments

We first illustrate the GVF fields generation on a noisy image in Fig. 5. For comparison, the GVF fields of this noisy image calculated by (1) are shown in Fig. 5(b), while the gradient flow $I_{\eta\eta}$ calculated directly from the observed image is shown in Fig. 5(c). The factor μ in (1) is empirically set to 0.5. It can be noted that the GVF flow fields appear smooth and many insignificant noise points can be effectively overcome in Fig. 5(b), while the gradient flow fields in Fig. 5(c) appear more disorderly. It is more sensitive to noise than the GVF flow fields. If applying (3) to approximate the gradient flow fields as shown in Fig. 5(d) (i.e., $I_{\eta\eta} \approx \vec{v} \cdot \mathbf{N}$), we note that the GVF-based gradient flow fields likewise behave in a disorderly manner. This is caused by the intensity normal vector from the observed image. Nevertheless, the boundaries of object are still preserved, and the evolution trend of the GVF flow field is not changed.

Subsequently, we illustrate the GVF-based shock filter on a mammographic image in Fig. 6(a)–(c). To deblur such noisy
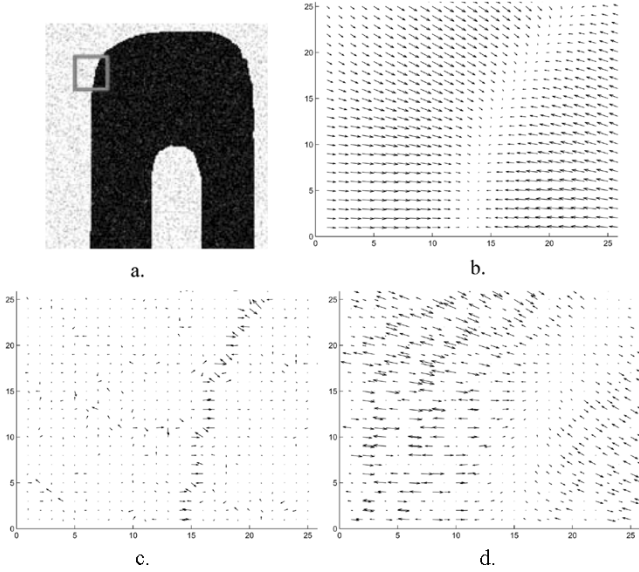
Fig. 5. GVF field of a noisy image (b–d flow fields corresponding to the rectangle of the noisy image), (a) noisy image, (b) GVF flow field, (c) gradient flow field without GVF, (d) GVF-based gradient flow field.

Fig. 6.   Evolutions of shock filter and mean curvature flow scheme. (a) Original image. (b) By the original shock filter. (c) By the scheme of (4). (d) MAD diagram of the shock filter.

and blurry medical images, the shock filter is applied as a stable deconvolution filter. By comparison, the experimental result of the original shock filter is also shown. It is noticed that the original shock filter overenhanced the details in Fig. 6(b), while the scheme of (4) is able to enhance the essential structures while suppressing trivial details. This is shown in Fig. 6(c). Fig. 6(d) demonstrates that the scheme of (4) can reach a steady-state solution more quickly than the original scheme with the mean absolute difference (MAD), which is calculated as $R(t) = (1/(M \times N)) \sum_{i,j}^{M,N} \left| I_{i,j}^{(t)} - I_{i,j}^{(0)} \right|$, where M and N are the width and height of the image, respectively. (All of the following experiments will adopt this MAD formula to generate the MAD diagrams.)

The original mean curvature flow and the proposed scheme of (5) are illustrated on a noisy and blurry image in Fig. 7(a)–(d), respectively. The original image is degraded with Gaussian noise (zero mean, with 0.1 variance), and then blurred by a Gaussian lowpass filter with variance $\sigma = 0.25$. We adopted $I_t = \kappa|\nabla I|$ as the original mean curvature flow scheme, and set $r = 0.5$ in the scheme of (5). It can be observed that the features of the water lily image are enhanced and denoised effectively by the scheme of (5) in Fig. 7(d), while all of the features are smoothed out gradually by the original scheme in Fig. 7(c). The MAD diagram in Fig. 7(e) demonstrates that the scheme of (5) is able to reach a steady-state solution and preserve the essential structure of shapes, while the original curvature flow scheme would eventually smooth out all of the information.

In the experiments for the P–M equation, the original scheme is compared with the proposed scheme of (6). The original water lily image is degraded with Gaussian noise and blurred as shown in Fig. 7(b). The diffusion results are shown in Fig. 8(a) and (b). Their diffusion effects seem to be close, but the MAD diagram in Fig. 8(c) demonstrates that the scheme of (6) is able to reach a steady-state solution more quickly than the original P–M equation.
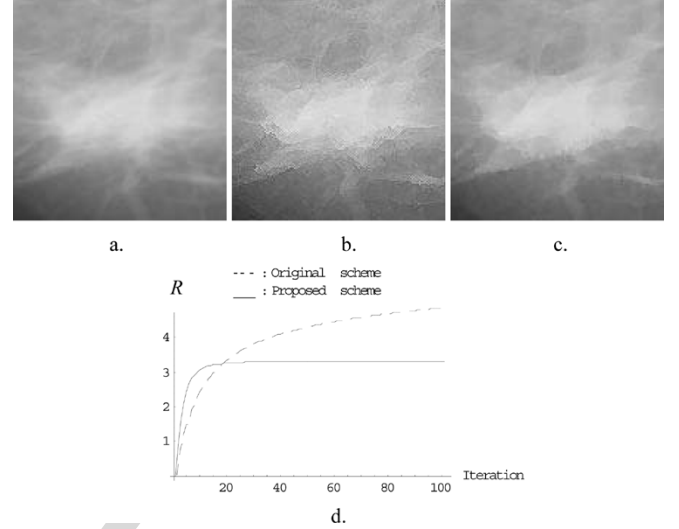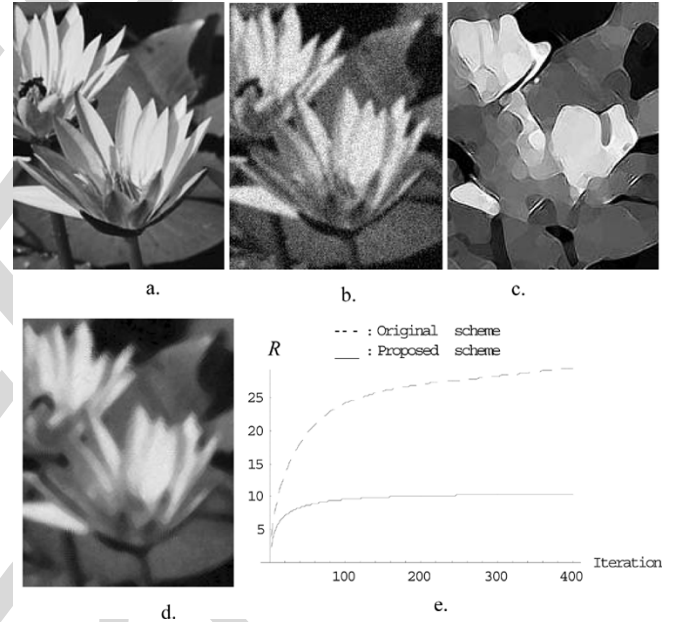
Fig. 7.   Evolutions of mean curvature flow scheme. (a) Original image. (b) Noisy and blurry image. (c) By original scheme. d) By scheme of (5). (e) MAD diagram of the mean curvature flow.

In the successive experiments, the scheme of (7) is demonstrated on the water lily image, which is blurred and degraded with Gaussian noise as illustrated in Fig. 7(b). The experimental results are shown in Fig. 9. It can be noted that when the coefficient m increases, some details with large gradients are enhanced, while others with small gradients are eroded gradually. This is due to the fact that the center of the inverse diffusion term in the scheme of (7) moves along with the change in the coefficient m.

In the experiment for the fourth-order flow scheme, the scheme of (9) is illustrated on the noisy and blurry water-lily image as shown in Fig. 7(b). The factor β is empirically set to 0.5 in (9). The result is compared with that of the scheme of (6) and depicted in Fig. 10. Due to the intrinsic Laplacian of

a.   b.
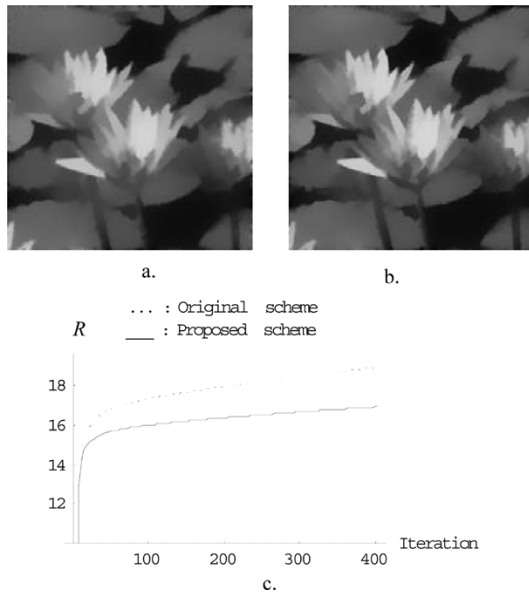
Fig. 8. Evolutions of the P-M equation with $\sigma_E = 0.45$. (a) By the original scheme with iteration $= 150$. (b) By the scheme of (6) with iteration $= 200$. (c) MAD diagram.

a.   b.   c.   d.
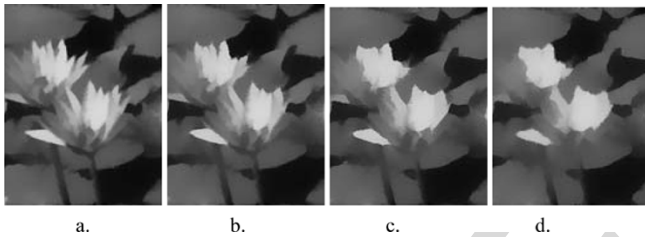
Fig. 9. Evolutions of the scheme of (7) with $\sigma_E = 0.45$, $s = 1$ and iteration $= 200$. (a) $m = 1$. (b) $m = 2$. (c) $m = 3$. (d) $m = 4$.

curvature term in (9), the boundaries of objects become distinct in Fig. 10(b). This indicates that the isoperimetric property from the intrinsic Laplacian of curvature term would enhance, while smoothing the shape boundaries during the image anisotropic diffusion.

V. Conclusion

In this paper, we first introduced the GVF fields in the image anisotropic diffusion. Some well-known nonlinear PDE models, such as the shock filter, the mean curvature flow, and the P-M diffusion model were reformulated based on the GVF fields. The particular advantages that the GVF brings about are the robust estimation of the high-order derivative, improvement of numerical stability, and the ability to perform well on noisy images. In addition, the proposed GVF-based anisotropic diffusion models are able to reach steady-state solutions more quickly than the original ones. In order to enhance and smooth the boundaries of an object without eroding them, the intrinsic Laplacian of the curvature is introduced in the anisotropic diffusion of images. Since this flow contains a fourth-order derivative term, it is very sensitive to image noise and computational errors. Despite this, we are able to obtain a robust estimate of this flow from the GVF fields. The experiments indicate that our proposed models are robust and practical as they exploit the GVF fields.

a.   b.
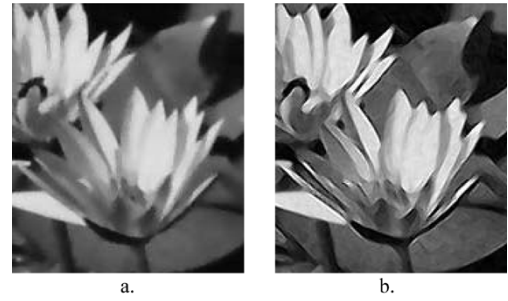
Fig. 10. Evolution of schemes (6) and (9) on the water lily image at iteration $= 200$. (a) By scheme (6). (b) By scheme (9).

For future work, the GVF-based P–M diffusion equation needs to be further examined. The design of the coefficient in the inverse diffusion term is also a critical problem to be investigated. In addition, we will apply these proposed diffusion models to a 3-D volume dataset for medical visualization, as the classification process is critical for direct volume rendering, with the anisotropic diffusion providing the desired classification results.

References

[1] P. Perona and J. Malik, "Scale-space and edge detection using anisotropic diffusion," *IEEE Trans. Pattern Anal. Mach. Intell.*, vol. 12, no. 7, pp. 629–639, Jul. 1990.

[2] L. Alvarez and L. Mazorra, "Signal and image restoration using shock filters and anisotropic diffusion," *SIAM J. Numer. Anal.*, vol. 31, no. 2, pp. 590–605, 1994.

[3] P. Kornprobst, R. Deriche, and G. Aubert, "Image coupling, restoration and enhancement via PDE's," in *Proc. Int. Conf. Image Processing*, Santa Barbara, CA, 1997, pp. 458–461.

[4] G. Gilboa, N. A. Sochen, and Y. Y. Zeevi *et al.*, "Regularized shock filters and complex diffusion," in *Proc. Europe Conf. Computer Vision*, vol. LNCS-2350, A. Heyden *et al.*, Eds., 2002, pp. 399–413.

[5] ——, "Forward-and-backward diffusion processes for adaptive image enhancement and denoising," *IEEE Trans. Image Process.*, vol. 11, no. 7, pp. 689–703, Jul. 2002.

[6] R. A. Carmona and S. Zhong, "Adaptive smoothing respecting feature directions," *IEEE Trans. Image Process.*, vol. 7, no. 3, pp. 353–358, Mar. 1998.

[7] A. Marquina and S. Osher, "Explicit algorithms for a new time dependent model based on level set motion for nonlinear deblurring and noise removal," *SIAM J. Sci. Comput.*, vol. 22, no. 2, pp. 387–405, 2000.

[8] L. Alvarez, F. Guichard, P.-L. Lions, and J.-M. Morel, "Axioms and fundamental equation of image processing," in *Archive for Rational Mechanics and Analysis*. New York: Springer-Verlag, 1993, vol. 123, pp. 199–257.

[9] J. Weickert, B. Romeny, and M. A. Viergever, "Efficient and reliable schemes for nonlinear diffusion filtering," *IEEE Trans. Image Process.*, vol. 7, no. 3, pp. 398–409, Mar. 1998.

[10] R. Malladi and J. A. Sethian, "A unified approach to noise removal, image enhancement and shape recovery," *IEEE Trans. Image Process.*, vol. 5, no. 11, pp. 1554–1568, Nov. 1996.

[11] C. Xu and J. L. Prince, "Snake, shapes and gradient vector flow," *IEEE Trans. Image Process.*, vol. 7, no. 3, pp. 359–369, Mar. 1998.

[12] S. Osher and L. Rudin, "Feature-oriented image enhancement using shock filters," *SIAM J. Numer. Anal.*, vol. 27, pp. 919–940, 1990.

[13] A. Polden, "Curves and surfaces of least total curvature and fourth-order flows," Ph.D. dissertation, Univ. Tubingen, **AUTHOR: PLEASE PROVIDE CITY AND DEPT.** , Germany, 1996.

[14] N. Paragios, O. Mellina-Gottardo, and V. Ramesh, "Gradient vector flow fast geodesic active contours," *IEEE Trans. Pattern Anal. Mach. Intell.*, vol. 26, no. 3, pp. 402–407, Mar. 2004.

[15] J. A. Sethian, *Level Set Methods and Fast Matching Methods*. Cambridge, U.K.: Cambridge Univ. Press, 1999.

[16] L. Alvarez, P.-L. Lions, and J.-M. Morel, "Image selective smoothing and edge detection by nonlinear diffusion II," *SIAM J. Numer. Anal.*, vol. 29, no. 3, pp. 845–866, 1992.

[17] N. J. Lott and D. I. Pullin, "Method for fairing B-spline surfaces," *Comput. Aided Design*, vol. 20, no. 10, pp. 597–604, 1988.

[18] C. Xu, J. L. Prince, and A. Yezzi, "A summary of geometric level-set analogues for a general class of parametric active contour and surface models," in *Proc. 1st IEEE Workshop Variational Level Set Methods in Computer Vision*, Vancouver, BC, Canada, 2001, pp. 104–111.

[19] G. Taubin, "A signal processing approach to fair surface design," in *Proc. SIGGRAPH*, Los Angeles, CA, 1995, pp. 351–358.

[20] M. Desbrun *et al.*, "Implicit fairing of irregular meshes diffusion and curvature flow," in *Proc. SIGGRAPH*, Los Angeles, CA, 1999, pp. 317–324.

[21] D. L. Chopp and J. A. Sethian, "Motion by intrinsic Laplacian of curvature," in *Interfaces and Free Boundaries*. Oxford, U.K.: Oxford Univ. Press, 1999, vol. 1, pp. 1–18.

[22] C. Xu and J. L. Prince, "Gradient vector flow deformable models," in *Handbook of Medical Imaging*, I. Bankman, Ed. New York: Academic, 2000.

[23] F. Catte, P.-L. Lions, J.-M. Morel, and T. Coll, "Image selective smoothing and edge detection by nonlinear diffusion," *SIAM J. Numer. Anal.*, vol. 29, pp. 182–193, 1992.

[24] T. Tasdizen, R. Whitaker, P. Burchard, and S. Osher, "Geometric surface smoothing via anisotropic diffusion of normals," in *Proc. IEEE Conf. Visualization*, Boston, MA, 2002, pp. 125–132.

Hongchuan Yu (M AUTHOR: PLEASE PROVIDE MEMBER YEAR received the Ph.D. degree in computer engineering from the Institute of Intelligent Machine, Chinese Academy of Science, **AUTHOR: PLEASE PROVIDE CITY** China, in 2000.

Currently, he is a Research Associate with the University of Western Australia, Perth, Australia. His research interests include medical imaging, motion estimation and tracking, and invariant pattern recognition.

Chin-Seng Chua (M'95) received the Ph.D. degree in computer vision from Monash University, **AUTHOR: PLEASE PROVIDE CITY**, Australia, in 1995.

Currently, he is a Faculty Member with Nanyang Technological University, Singapore. From 1995 to 1997, he was with the Defence Science Organization. His research interests include computer vision, face recognition, and visual surveillance.